# Fatigue crack growth in steel beams strengthened by CFRP strips

Pierluigi Colombi *, Giulia Fava

*Department of Architecture, Built Environment and Construction Engineering, ABC, Politecnico di Milano, P.zza L. da Vinci, 32, 20133 Milan, Italy*

The present paper investigates the fatigue crack growth of steel beams strengthened by using Carbon Fibre Reinforced Polymers (CFRP) from the experimental and analytical point of view. Artificially cracked steel beams were reinforced at the bottom side of the tension flange by applying CFRP strips bonded with epoxy adhesive. Different reinforcement arrangements were considered (i.e., single and double reinforce-ment layer) and the specimens were tested under a four-point bending configuration. Then, an analytical model was proposed to predict the strain redistribution in the reinforcement strips and the fatigue crack growth curves. Experimental evidence showed the presence of a debonded area between the reinforcement and the steel beam at the crack location. In detail, for the double reinforcement case, this caused a noticeable scatter of the fatigue crack growth curves. Finally, a good agreement was found between the analytical results and the experimental ones, in terms of both the strain distribution in the CFRP and fatigue crack growth curves.

*Keywords:*
Steel beams
Bonded CFRP strips
Debonding
Experimental analysis

## 1. Introduction

When steel structures are subjected to repeated loads, fatigue failure may commonly occur. Such a phenomenon is typical for steel structures in the civil engineering field as roads and railway bridges, towers, tanks, pipelines and crane supporting structures. Besides, fatigue loading in stress concentration zones can lead to crack nucleation and growth and finally to the complete failure of the structural element. Concerning the fatigue failure of steel beams, several repair techniques may be considered to extend the fatigue finite life of the structural element (fatigue lifetime). In detail, in old metallic structures close to the design fatigue life, defects should be repaired to prolong the fatigue lifetime. On the other hand, when there are no existing defects, crack initiation should be prevented to maintain the structural members in the ‘‘infinite life” regime.

Efficient repair techniques are then required to retrofit existing steel structures under cyclic loads. Traditional techniques [1] such as welding or steel plate bolting are not effective as they may introduce additional stress concentration zones and eventually increase the self-weight of the structure. Moreover, they are time consuming and costly. All these disadvantages can be mitigated by applying composite materials such as the Carbon Fibre Reinforced Polymers (CFRP). Such a reinforcing strategy was already shown to be effective in several state-of-the-art reports [2–5]. Guidelines are also available [6,7] for the design of CFRP repaired steel structures. Composites have unique material and mechanical properties such as low self-weight, high strength and stiffness, good durability. Despite the high material cost, due to the composite materials qualities, the strengthening operations are quickly realized and the global rehabilitation charges are therefore reduced. Such a reinforcing technique is quite attractive for the flexural strengthening at the ultimate limit state (when the elastic structural response is not significantly improved), the strengthening against local buckling, the confinement of hollow steel tubes and mainly for the fatigue reinforcement [5].

Failure mode of CFRP reinforced steel elements is usually due to interface failure occurring at the steel–adhesive interface. Moreover, the adhesive joint is sensitive to high temperature, water and moisture exposure. Galvanic corrosion is also a potential prob-lem since, when the carbon fibres come in contact with the steel surface, a galvanic cell is obtained. On the other hand, FRP reinforcement cannot be efficiently applied to a non-smooth surface. This is the case with riveted girders, due to the high rivet density. Besides, for heritage structures, reversibility of the strengthening system is highly recommended and bonded FRP materials cannot be easily removed from the steel surface.

### 1.1. Problem statement

With specific reference to fatigue damaged structures, CFRP reinforcements can reduce crack growth and extend the fatigue life acting in three different ways:

* Corresponding author. Tel.: +39 0223994280.
*E-mail address:* pierluigi.colombi@polimi.it (P. Colombi).


Published Journal Article available at: http://dx.doi.org/10.1016/j.tafmec.2016.01.007

- by reducing the effective stress range around the crack tip;
- by reducing the crack opening displacement (COD); i.e. CFRP materials bonded to the crack bridge the crack lips and moderate the COD;
- by promoting crack closure.

Regarding the last point, as the crack propagates, a plastic deformation zone is left in the wake of the advancing crack tip and the permanent elongations are not recovered as the load is released to the minimum level. Then premature contact between the crack lips occurs, leading to the crack closure phenomenon at a load level greater than the minimum one. The application of a reinforcement strip reduces the crack opening displacement and thus promotes crack closure.

It is then evident that the reinforcement stiffness plays a very important role in the fatigue reinforcement of steel elements. High stiffness reinforcing materials result, in fact, in a significant decrease of the stress range around the crack tip and in a marked reduction of the COD which promotes crack closure. Crack closure is also emphasized when CFRP strips are prestressed, since the compressive stresses reduce the load ratio and the crack closure is promoted. On the other hand, in cracked steel elements a severe stress and strain concentration exists close to the defect. Thus, crack induced debonding may occur and it is not possible to elude it either by a proper reinforcement curtailment or by mechanical anchorage. Such a debonded region has a significant influence on the fatigue crack propagation since it lessens the effect of the reinforcing strips.

### *1.2. Previous studies*

Research activities on the efficacy of the fatigue repair in cracked steel beams are summarized below.

Nozaka et al. [8] analysed different combinations of two CFRP reinforcements and five adhesive types for the rehabilitation of cracked steel girders subjected to fatigue. It was observed that the better fatigue performance was attained by using the CFRP and adhesive type with the lowest moduli of elasticity.

Deng and Lee [9] considered the fatigue behaviour of 1.2 m long steel beams retrofitted with CFRP strips. During the tests, the crack initiation and progressive growth along the CFRP reinforcement were monitored. Finally, a stress–fatigue life ($S$–$N$) curve was obtained.

More recently, Ghafoori and Motavalli [10] described and validated an analytical model based on the approach of crack surface widening energy release rate. They aimed to calculate the stress intensity factor for cracked steel I-beams. For a cracked beam under cyclic loading, the fatigue crack growth rate, residual deflec-tion and stiffness reduction were analysed.

In [11] the flexural behaviour of damaged steel beams repaired with CFRP strips was considered. Static and fatigue tests were performed and finite element analyses were conducted to predict the experimental behaviour. Strain-life method and cumulated damage theory were used to simulate the fatigue response of the repaired beams.

In [12], based on the outcomes of an experimental program, the behaviour of notched steel beams repaired with CFRP materials was studied. Different levels of initial damage (i.e. notch depth) were considered in order to investigate multiple stages of fatigue crack propagation in a steel beam. A numerical model was pro-posed to simultaneously take into account both the crack propaga-tion in the steel section and the debonding of the CFRP reinforcement from the steel substrate. Results showed that the initial damage level significantly affected the steel beams behaviour and the CFRP debonding. In [13], a numerical model for the stress intensity factor evaluation of a cracked steel I-beam was additionally provided.

In [14], the interaction between the CFRP reinforcement and the level of damage in the steel beam was presented. An experimental campaign was conducted and finite element analyses were executed to predict the experimental results. Local debonding of the CFRP strips was observed at the damage location due to stress concentration. The level of initial damage influenced debonding propagation rate of the CFRP.

Ghafoori et al. [15] analysed the fatigue behaviour of notched steel beams reinforced with non-prestressed and prestressed CFRP patches, with specific attention to the effect of crack propagation and FRP-to-steel debonding on the fatigue crack growth rate. In [16], experimental findings and a theoretical study were presented on the behaviour of notched steel beams reinforced by using non-prestressed and prestressed CFRP strips. A fracture mechanics model was proposed for the estimation of the required prestressing level needed to stop the crack propagation in the notched beams.

In [17], the flexural behaviour of notched steel beams repaired with CFRP strips was presented. A model was proposed and experimentally validated to examine the effects of CFRP repair taking into account the bond-slip behaviour of CFRP-steel interface. A parametric analysis was performed with respect to various engineering properties of CFRP materials and adhesives. The analyses confirmed the improved effectiveness of high modulus reinforcement in affecting repairs of steel elements.

Wu et al. [18] conducted an experimental program for the definition of the fatigue behaviour in artificially notched steel beams strengthened with four different reinforcement types and then tested under equivalent tensile stiffness. It was observed that composite materials did not only postpone crack initiation, moderate the crack growth rate and increase the fatigue life, but also lessened the stiffness decay and residual deflection.

Ghafoori et al. [19] presented a design criterion to evaluate the prestress level for avoiding fatigue crack in steel beams reinforced by using CFRP strips. Constant life diagrams were used to determine the minimum level of CFRP pre-stress required for extending the fatigue life of existing metallic beams. It was also shown that the application of a compressive force by using pre-stressed CFRP plates led to a reduction of the mean stress level such that the detail was shifted from the ‘finite life’ regime to the ‘infinite life’ regime. In [20] a design criterion was also presented for fatigue strengthening of a 120-year-old metallic railway bridge in Switzerland. Both prestressed bonded and un-bonded CFRP reinforcement were investigated. The paper illustrated an application of the constant life diagrams concept [19] for estimating the minimum CFRP pre-stress level required to prevent fatigue crack initiation.

It is commonly observed that the use of CFRP reinforcements increases the fatigue life and reduces the crack growth rate. As the strength of the steel substrate is very high, in the CFRP rein-forced steel member, the adhesive layer represents the weakest link and the dominant failure mode is the CFRP debonding. For fati-gue strengthening, the presence of a debonded region close to the crack location, noticeably diminishes the efficacy of the strength-ening method and should be considered when the fatigue lifetime is estimated. This study meets the need of additional and well-documented experiments in such a research topic, as expressed in [21].

### *1.3. Scope of the research*

In this work, the crack growth of CFRP strengthened steel beams is investigated from both the experimental and analytical point of view. Artificially cracked steel beams were strengthened by applying CFRP strips that were bonded to the bottom side of the tension

flange. The initial crack was shaped by notching the tension flange and part of the web of the beam. Four-point bending tests were conducted under constant amplitude cyclic loads. The influence of two different reinforcement thicknesses was also investigated. During the test execution, a debonded zone was observed at crack location, due to the high stress/strain concentration [22]. As debonding is known to have a detrimental effect on the reinforcement, it was taken into account in analysing the fatigue behaviour. In fact, while the influence due to CFRP debonding was well documented for steel plates reinforced by CFRP strips [23], information is still incomplete for the case of repaired steel beams.

In order to define how a debonded area close to the crack may influence the fatigue crack propagation and to examine the debonding shape effects on the crack propagation curves, strain gauges were positioned on the tensile flange of some beams.

So far, there had been few attempts to analyse from the numerical point of view the mutual influence of the fatigue crack propagation and the reinforcement debonding [11,14,17]. Additionally, only few analytical and numerical models were developed to predict the fatigue behaviour in steel beams repaired with CFRP composites [10,13]. Therefore, for the first time in the literature, in this work an analytical model is illustrated in order to define and compute the fatigue crack propagation rate and then the fatigue lifetime, accounting also for the effect of reinforcement debonding.

## 2. Experimental program

### 2.1. Test program

Details of the experimental program are provided in Table 1.

In particular, pultruded CFRP strips were bonded on nine cracked steel beams and the reinforced specimens were subjected to fatigue loading at the laboratories of the Politecnico di Milano. The reinforced beam geometry is provided in Fig. 1(a), while the section and notch details are shown in Fig. 1(b) and (c), respectively.

In the experimental program, I-shaped steel beams (IPE 120 according to European standard EN 10025) were used. The beams were artificially cracked and reinforced by applying CFRP strips to investigate the strengthening effectiveness. Specimens were artificially notched at the midspan section through the tension flange and a part of the web. In detail, the damage in the beams was firstly created with a 2.5 mm thick and 16 mm long blade saw cut in the flange and web and then with a supplementary 1 mm thick and 2 mm long hand saw cut in the web. The additional 2 mm long saw cut was shaped to produce a more severe stress concentration and to support the fatigue crack propagation verti-cally in the web. The reinforced beams were then subjected to fatigue loads in order to create a further crack increment of 2 mm. Thus, the initial crack size was in total of 20 mm, as illustrated in Fig. 1(c).

**Table 1**
Details of the experimental program and test.

| Specimen | $a_i$ (mm) | $t_c$ (mm) | $\Delta F$ (kN) | $a_f$ (mm) | $N_f$ (–) |
|---|---|---|---|---|---|
| B01 | 20 | / | 6–15 (10 Hz) | 60 | 233,500 |
| B02 | 20 | 1.4 | 6–15 (10 Hz) | 20 | 280,000 |
| B03[a] | 20 | 1.4 | 28–70 (3 Hz) | 60 | 19,700 |
| B04 | 20 | 1.4 | 28–70 (3 Hz) | 60.9 | 24,000 |
| B05 | 20 | 2.8 | 28–70 (3 Hz) | 60.4 | 183,000 |
| B06 | 20 | 2.8 | 28–70 (3 Hz) | 60.9 | 114,000 |
| B07 | 20 | 2.8 | 28–70 (3 Hz) | 60.4 | 228,000 |
| B08 | 20 | 2.8 | 28–70 (3 Hz) | 60.2 | 180,000 |
| B09 | 20 | 2.8 | 28–70 (3 Hz) | 35 | 185,000 |

$a_i$ = initial crack size.
$t_c$ = reinforcement thickness.
$\Delta F$ = load range applied to the spreader beam.
$a_f$ = final crack size.
$N_f$ = number of cycles from $a_i$ to $a_f$.
[a] Retested.

The notched beams were reinforced by applying CFRP strips (Sika CarboDur® M614) where the thickness, width and length are respectively equal to 1.4 mm, 60 mm and 800 mm. The nomi-nal values (5% fractile-value) of the Young's modulus and tensile strength were equal to 205 GPa and 3200 MPa, as reported in the technical datasheet. The steel beams were strengthened according to the following procedure. The bottom side of the tension flange was accurately grid blasted with an abrasive disc to remove the rust and create a rough surface. For improving the bond strength, the surface roughness of the CFRP strip was increased by using very fine sandpaper (grit P240). The surfaces were then accurately cleaned for promoting the mechanical interlocking. An epoxy adhesive (Sikadur® 30) was used to bond the composite to the bottom side of the tensile flange. The average adhesive thickness was of 2.5 mm. For specimens reinforced with two composite layers, another type of epoxy adhesive (Sikadur® 330) was distributed on the previously applied CFRP reinforcement, and the second strips were pressed. The mechanical properties of the steel and CFRP strip were determined through the execution of tensile tests. Details concerning the materials mechanical properties are listed in Table 2.

At first, the bare specimen B01 and the reinforced beam B02 were tested under a fatigue loading ranging from $P_{min}$ = 6 kN to $P_{max}$ = 15 kN and at a frequency of 10 Hz. The fatigue load range corresponds to a load ratio $R$ = 0.4 and it was selected to reproduce a severe fatigue situation. In fact, at such a loading ratio, the retardation effects are reduced and then the fatigue crack propagation is likely to advance more rapidly.

For specimens B03–B09, the designated maximum fatigue loading, $P_{max}$ = 70 kN, corresponded to a mid-span bending moment $M$ equal to 8.75 kN m, which was about 50% of the yielding bending moment of the un-cracked beam section, $M_y$ = 17.78 kN m. The minimum load, $P_{min}$, was equal to 28 kN, resulting again in a load ratio $R$ = 0.4. The loading frequency was equal to 2 Hz.

### 2.2. Measuring and recording equipment

All beams were tested under a four-point bending configuration over a simply supported span of 1000 mm (see Fig. 2a).

When the fatigue tests were carried on, it was fundamental to record the crack growth development with respect to the fatigue cycles. A piece of graph paper was positioned on the beam web close to the ligament (see Fig. 2b) and a travelling microscope with a magnifying power up to 220× was used to measure the crack growth at intervals from 500 to 10,000 cycles, depending on the crack front speed.

In reinforced beams B04, B06, B07 and B09, the CFRP reinforcements were instrumented with 8 strain gauges close to midspan, in order to investigate the tensile strain distributions along the composite and to monitor the progressive debonding propagation of the CFRP strip close to the notch (Fig. 3).

## 3. Analytical modelling

### 3.1. Fatigue crack growth law

Linear elastic fracture mechanics concepts were used to explore the fatigue crack growth. Specifically, based on the Paris law, the crack growth rate was calculated. In this study, the following modified version of the Paris law was proposed [23]:

$$\frac{da}{dN} = C \cdot \left(\Delta K_{eff}^{m} - \Delta K_{eff,th}^{m}\right) \quad (1)$$

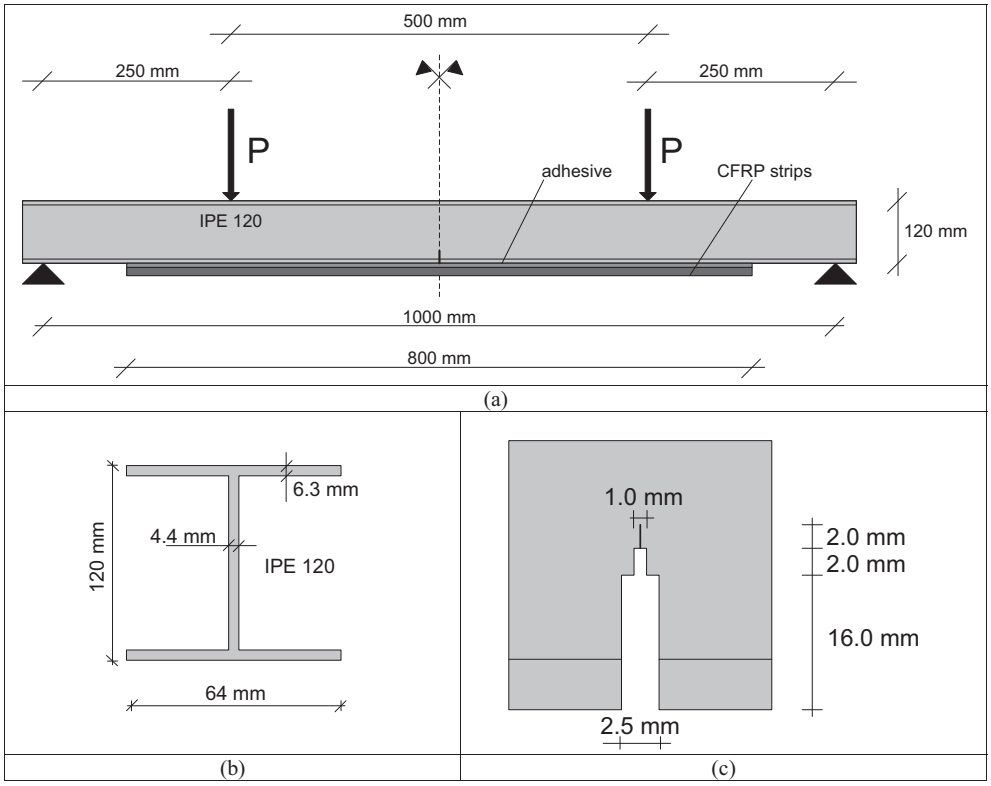


**Fig. 1.** Specimen geometry: (a) experimental beam geometry, (b) beam section and (c) notch details (not to scale).

**Table 2**
Material mechanical properties.

| | Young's modulus (GPa) | Yield stress (MPa) | Tensile strength (MPa) | Pot life (min) |
|---|---|---|---|---|
| Steel | 208 | 330 | 444 | – |
| CFRP | 195 | – | >2800 | – |
| Adhesive (Sikadur® 30) | >4.5 | – | >28.4 | 70 |
| Adhesive (Sikadur® 330) | >3.8 | – | >30.0 | 30 |

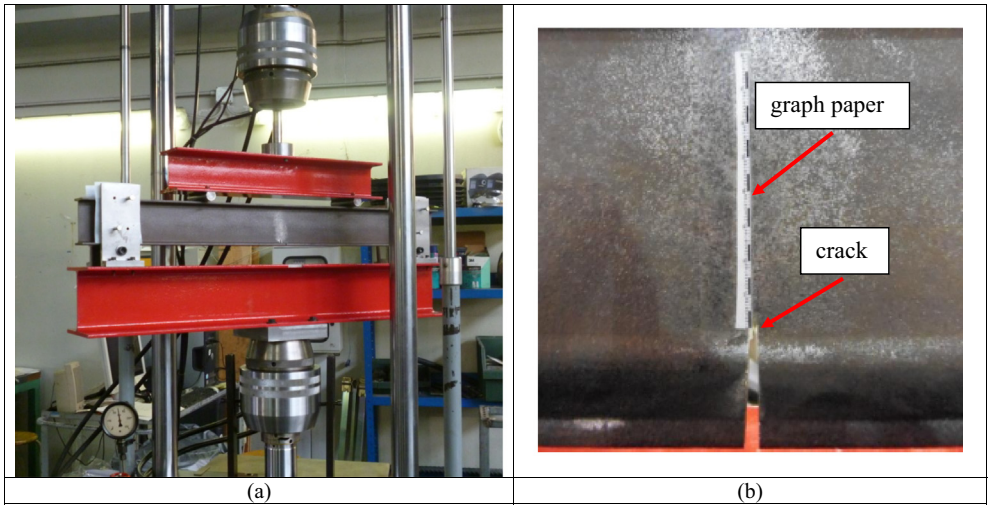


**Fig. 2.** Experimental set-up and measuring system: (a) four-point bending test and (b) crack measurement.

In Eq. (1) $a$ is the crack size, $N$ is the number of duty cycles, $\Delta K_{eff}$ is the effective SIF range, $\Delta K_{eff,th}$ is the effective threshold SIF range and $C$ and $m$ are material parameters (Paris constants). The crack growth rate is presumed to be equal to zero (no crack growth) for stress ranges lower than the threshold stress range, i.e., if the stress range is lower than the threshold stress range, no crack propagation occurs. Besides, the crack experiences crack closure during the fatigue life, that is, the premature contact of the crack


**Fig. 3.** Strain gauges layout and positioning on the CFRP reinforcement.

face is reached during the unloading branch of the duty cycle. It is therefore assumed that the crack does not act as stress concentrator if the stress is lower than the so called opening stress. Only when the opening stress is achieved, the crack becomes fully opened and the fatigue crack propagation may take place. This means that only a part of the stress range, the so called effective stress range, is then effective for crack propagation. The effective SIF range, $\Delta K_{eff}$, is described as:

$$\Delta K_{eff} = K_{max} - K_{op} = (1 - q) \cdot K_{max} \tag{2}$$

where $q$ is the effective load ratio:

$$q = \frac{M_{op}}{M_{max}} \tag{3}$$

and $K_{op}$ is the opening SIF, i.e. the SIF level when the crack completely opens. The effective load ratio, $q$, is calculated by using the following expression [23]:

$$q = \beta \cdot \max\left[\frac{1}{1 + pcf}(1 + R \cdot R_{ys}), R\right] \tag{4}$$

where $R = M_{min}/M_{max}$ is the load ratio, $R_{ys} = M_{max}/M_y$ is the yield load ratio ($M_y$ is the yield bending moment) and $pcf$ is the plastic constraint factor. In the case under investigation one had $R_{ys} = 0.49$. The plastic constraint factor takes into consideration the thickness effect on fatigue crack growth and ranges from 1 (plane stress condition) to 3 (plane strain condition). In this work, following [24], it was observed that experimentally determined plastic constraint factors are mostly between 1.5 and 2 and thus it was assumed $pcf = 1.68$. Additionally, in Eq. (4), $\beta$ is an experimental correction factor to be estimated from the experimental results as proposed in [23].

In [23], experimental data on the bare steel plate were considered for calibrating the parameters governing the fatigue crack propagation law (see Eq. (1)). In fact, for the steel plates used in [23] the steel quality was the same than the one of the steel beams considered in this work, i.e. S275 according to the European standard EN 10025. It was therefore expected that the fatigue crack growth parameters were the same. As Eqs. (1) and (4) held also for the cracked steel plates investigated in [23], the effective load ratio, $q = 0.46$, was calculated using Eq. (4) assuming $\beta = 1$.

In brief, in [23] the fatigue crack growth rate was determined from the experimental data as:

$$\left(\frac{da}{dN}\right)_{\bar{a}} = \frac{(a_{i+1} - a_i)}{(N_{i+1} - N_i)} \tag{5}$$

Then, after some algebra, the experimental effective SIF range was evaluated from Eq. (1) as:

$$\frac{1}{m}\left\{\log\left[\left(\frac{da}{dN}\right)_{\bar{a}} + C\Delta K_{eff,th}^{m}\right] - \log(C)\right\} = \log(\Delta K_{eff}) \tag{6}$$

At last, the non-linear least square method and the software MATLAB were employed for determining the best fit of parameters $C$, $m$ and $\Delta K_{eff,th}$ in Eq. (6) by assuming the average crack growth rate as independent variable and the effective SIF range as dependent variable. The results in terms of the unknown parameters are reported in Table 3.

Finally, the calibrated fatigue crack propagation law (see Eq. (1) and Table 2) is compared to experimental data in Fig. 4, where the data points refer to different measures taken from a unique fatigue test on a S275 bare steel plate [23], while the solid line is the relevant best fit.

### 3.2. Adhesion analysis

Under the assumption that linear interface behaviour was preserved up to failure, an analytical model was considered to estimate the stresses in the reinforcement and in the adhesive layer. The basic hypotheses were:

1. elastic stress–strain relationship for the steel and the composite and linear interface behaviour up to failure;
2. plane sections remain plane during bending;
3. stresses in the adhesive layer do not change with thickness; that is, the adhesive layer is thin;
4. the bending stiffness of the reinforced beam is much greater than the stiffness of CFRP strips.

Based on the last assumption, the bending moment in the CFRP strips and the normal stresses in the adhesive layer can be neglected when the tensile stress in the composite and the shear stress in the adhesive joint are estimated. Referring to the geometry of Fig. 5, the maximum shear stress in the adhesive layer was calculated as:

$$\tau_{max} = \frac{\lambda}{b_c}\left(N_{c0} - \frac{M}{f_2 E_s W_s}\right) \tag{7}$$

where

$$\lambda^2 = \frac{G_a b_c}{t_a}\left(\frac{1}{E_c A_c} + \frac{1}{E_s A_s} + \frac{h}{2E_s W_s}\right)$$
$$f_2 = \lambda^2 \frac{t_a}{G_a b_c} \tag{8}$$

and $E_c$, $A_c$ and $b_c$ are the composite section Young's modulus, section area and width, respectively. $E_s$, $A_s$ and $h$ are the steel section Young's modulus, section area, and height, respectively. $W_s$ is the steel resistance modulus and $G_a$ and $t_a$ are the adhesive shear modulus and thickness, respectively.

In Eq. (7), $N_{c0}$ and $M$ are the axial force in the reinforcement and the applied bending in the cracked section. Eq. (7) provides a relationship between the maximum shear stress and the tensile force

**Table 3**
Estimated fatigue crack growth parameters.

| $\Delta K_{th}$ (MPa $\sqrt{}$mm) | $C$ | $m$ |
|---|---|---|
| 161.8 | 2.669e−014 | 3.307 |

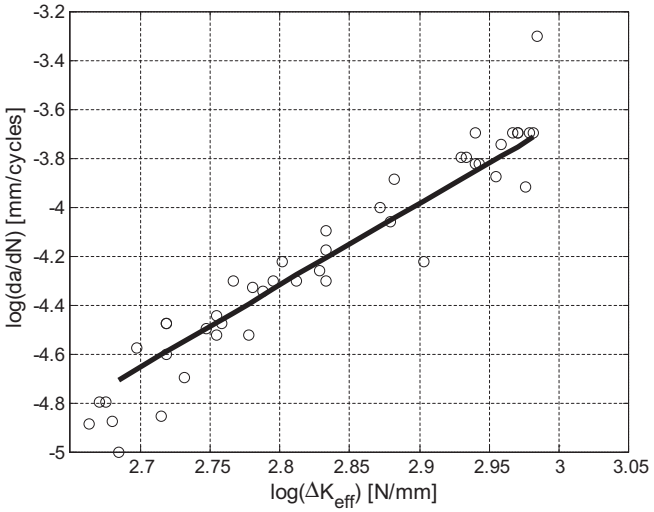


**Fig. 4.** Relationship between the crack growth rate and the effective stress intensity factor range for the bare steel plate.

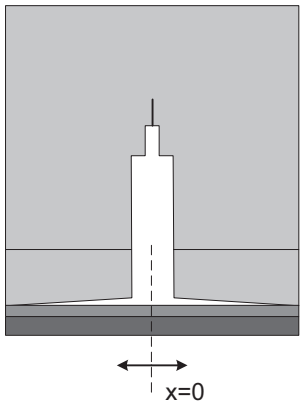


**Fig. 5.** Geometry of the cracked section at the mid-span: initial condition and reference axis.

$N_{c0}$ in the cracked section. In the reinforced beams, debonding at the cracked section is achieved when the maximum shear stress exceeds the allowable limit. In this sense, Eq. (7) provides a relationship for evaluating the relevant tensile force in the CFRP strip at the cracked section when debonding is present. Under this point of view, this analytical model can be regarded as a useful tool for estimating the debonding strength of the reinforced beams in the cracked section.

Eventually, the tensile force in the reinforcement layer can be estimated as:

$$N_c = \frac{M}{f_2 E_s W_s} + \left(N_{c0} - \frac{M}{f_2 E_s W_s}\right) e^{-\lambda x} \tag{9}$$

where the terms have the same meaning as in Eqs. (5) and (6) and $x$ is a local coordinate starting at the midspan (see Fig. 5). It is interesting to note that the first (constant) term in Eq. (9) corresponds to classical strength of materials solution that may be obtained using a standard transformed section approach.

### 3.3. Stress intensity factor evaluation

In [25] a simple formula was proposed to evaluate the stress intensity factor of an un-reinforced cracked I-beam. An alternative formulation based on FEM analyses was proposed in [13]. The formula was based on elementary beam-theory and made use of the energy release rate for crack widening concept. Under an external bending moment, the following formula was derived:

$$K_I^M = M\sqrt{\frac{\beta_M}{I_s \cdot t_w}\left(\frac{I_s}{I_{cr}} - 1\right)} \tag{10}$$

where $M$ is the bending moment, $I_s$ is the moment of inertia of the steel section, $I_{cr}$ is the moment of inertia of the cracked steel section and $t_w$ is the web thickness. In [10] the method was also extended to a beam under an external axial force and the following formula was proposed:

$$K_I^N = N\sqrt{\frac{\beta_N}{A_s \cdot t_w}\left(\frac{A_s}{A_{cr}} - 1\right)} \tag{11}$$

where $N$ is the axial force applied to the centroid of the cracked section, $A_s$ is the section area and $A_{cr}$ is the area of the cracked steel section. In Eqs. (8) and (9), $\beta_M$ and $\beta_N$ are non-dimensional functions depending on the crack length and beam geometry for pure bending and axial force, respectively. In this work it was assumed that $\beta_M = \beta_N$, while the following expression was proposed in [25] for $\beta_M$:

$$\begin{aligned} \beta_M &= \frac{1.16}{\psi^{0.374}} \\ \psi &= \frac{a}{h} \end{aligned} \tag{12}$$

Eqs. (8) and (9) could be used to evaluate the stress intensity factor of a reinforced steel beam in the following way. First, it should be noted that a compressive force, $N_b$, is applied to the steel beam:

$$N_b = -N_{c0} \tag{13}$$

where $N_{c0}$ is the CFRP axial force in the cracked section. Such a compressive force is clearly not applied to the centroid of cracked section and then an additional bending moment should be introduced to take into account the load eccentricity. The total bending moment, $M_b$, in the cracked section of the steel beam is then equal to:

$$M_b = M - N_{c0} \cdot y_c \tag{14}$$

where $M$ is the external bending moment and $y_c$ is the centroid position in the cracked steel section. The stress intensity factor, $K_I$, of the reinforced beam can be finally computed, inserting Eqs.(11) and (12) into Eqs. (8) and (9)), as:

$$K_I = (M - N_{c0} \cdot y_c)\sqrt{\frac{\beta_M}{I_s \cdot t_w}\left(\frac{I_s}{I_{cr}} - 1\right)} - N_{c0}\sqrt{\frac{\beta_N}{A_s \cdot t_w}\left(\frac{A_s}{A_{cr}} - 1\right)} \tag{15}$$

The strong influence of the axial compressive force on the stress intensity factor of the steel beam is evident from Eq. (15). The axial force and its associated bending moment reduce the stress intensity factor and the relevant crack opening displacement, promoting then crack closure.

## 4. Results and discussion

### 4.1. Strain distribution in the CFRP plate

Based on the analytical model proposed in the previous Section, both for one reinforcement layer and for two reinforcement layers, the debonding CFRP tensile force was estimated and compared to the corresponding value experimentally achieved. The axial force recorded at the midspan along the midline of the tension flange is plotted against the ratio $a/h$, i.e., the crack depth, $a$, normalized with respect to beam height, $h$, see Fig. 6.

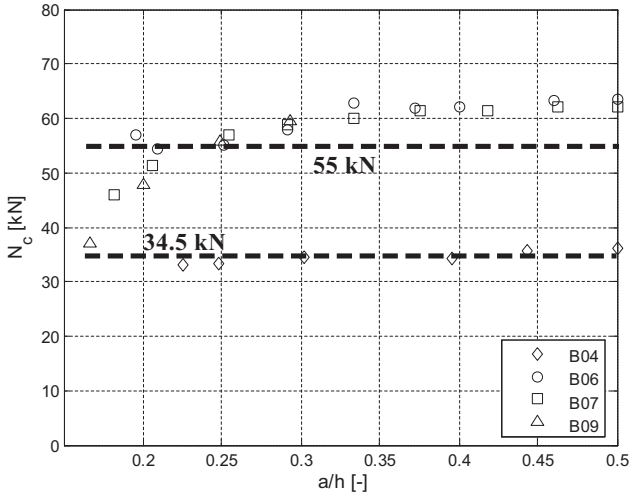


**Fig. 6.** Tensile force in the composite strip at the cracked section: experimental and analytical results for one reinforcement layer (specimen B04) and two reinforcement layers (specimen B06, B09 and B07).

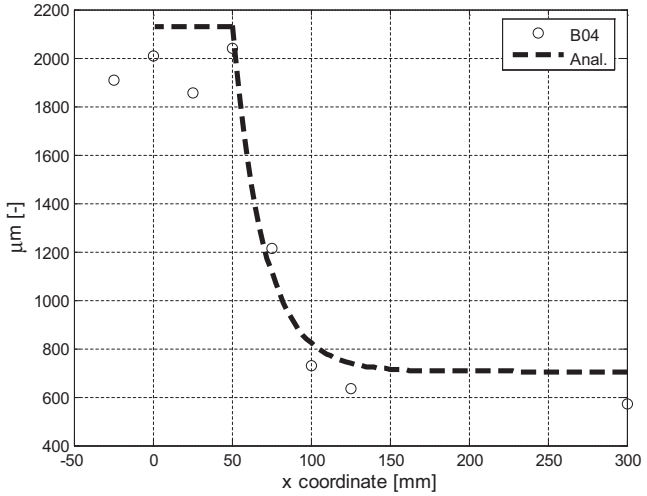


**Fig. 7.** Comparison of strain gauge measurements and analytical modelling of the reinforcement strain in specimen B04 ($a$ = 30.5 mm).

For specimens B04, B06, B07 and B09, the experimental results were obtained from the strain readings in the following way. At first, the microstrain, $\varepsilon_0$, at $x = 0$, was evaluated and then the tensile force in the CFRP strip was calculated as $N_c = \varepsilon_0 \cdot E_c \cdot A_c$, where $E_c$ is the Young's modulus of the reinforcement and $A_c$ is the composite section area. As clearly showed in Fig. 6, the axial force in the reinforcement layer was almost independent of the crack size. Besides, the axial force in the reinforcement at the midspan, $N_{c0}$, was assumed equal to the relevant debonding force and, based on Eq. (7), $N_{c0}$ was estimated as:

$$N_{c0} = \frac{b_c}{\lambda}\tau_{adm} + \frac{M}{f_2 E_s W_s} \tag{16}$$

In Eq. (16) the allowable adhesive shear stress $\tau_{adm}$ was required and it could be roughly estimated equal to 20 MPa according to [8,18]. Inserting this value in the Eq. (16), for an exter-nal bending moment of 8.75 kN m, a debonding CFRP tensile force of approximately 34.5 kN was achieved for a single reinforcement configuration. This value was in agreement with the CFRP tensile force experimentally obtained and reported in Fig. 6. Following the same procedure for a double reinforcement arrangement, a debonding CFRP tensile force equal to approximately 55 kN was obtained. In this case the analytical value provided a reasonable estimation of the tensile force in the CFRP reinforcement, as showed in Fig. 6. It is important to notice that for $a/h < 0.2$, the experimental axial force at the mid-span is not uniform. This means that for small crack sizes in the steel beam, the stress redistribution between the steel flange and the CFRP is reduced and a lower axial force is carried by the reinforcement. For small crack sizes, in fact, the beam stiffness is much larger than the reinforcement one and the stress redistribution occurs only in the first composite layer. As the crack length increases, the beam stiffness decreases and, as a result, both the reinforcement layers are involved in the stress redistribution. This has a strong influence on the fatigue crack growth as clearly evidenced by considering the experimental results.

In order to provide a further validation of the above assumption concerning the axial force redistribution at the CFRP midspan, for a single reinforcement configuration and a crack length $a$ equal to 30.5 mm, a typical strain distribution is reported in Fig. 7.

Fig. 8 provides a similar strain distribution for the double reinforcement arrangement and $a$ = 29.8 mm.

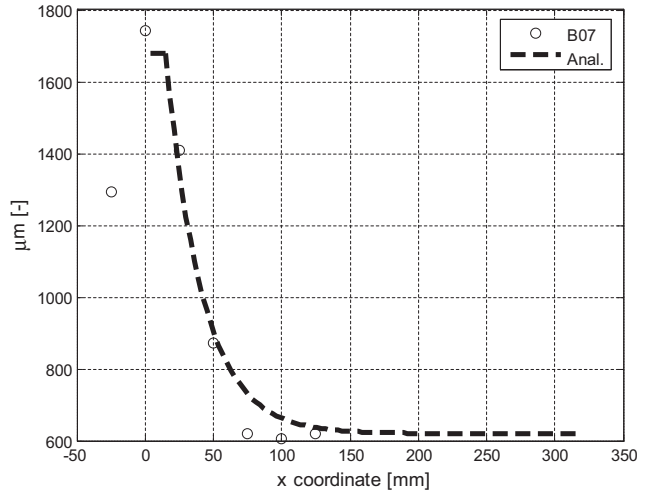


**Fig. 8.** Comparison of strain gauge measurements and analytical modelling of the reinforcement strain in specimen B07 ($a$ = 29.8 mm).

The plots in Figs. 7 and 8 were obtained as follows. At first, based on the experimental strain gauge readings, the tensile strain in the reinforcement was plotted and the plateau with constant strain values was roughly estimated. It was possible to notice that the tensile strain in the reinforcement was constant over a length of 50 mm in the case of a single reinforcement layer and over a length of 15 mm for two reinforcement layers. In Figs. 7 and 8, the plateau was followed by the analytical strain distribution cor-responding to the CFRP axial force of Eq. (9). On the other hand, the debonding force value was obtained from Eq. (16) and represented the initial axial force condition at the midspan. The axial strain was then obtained as $N_c/E_cA_c$. The agreement between the overall ana-lytical prediction and experimental findings was finally good both for the single and for the double reinforcement configuration.

### *4.2. Stress intensity factor in the reinforced beams*

In the case of a bare steel beam, the SIF was computed according to Eq. (10) for the maximum load level of 15 kN (see Table 1). In Fig. 9 the SIF was plotted with respect to the normalized crack length, $a/h$.

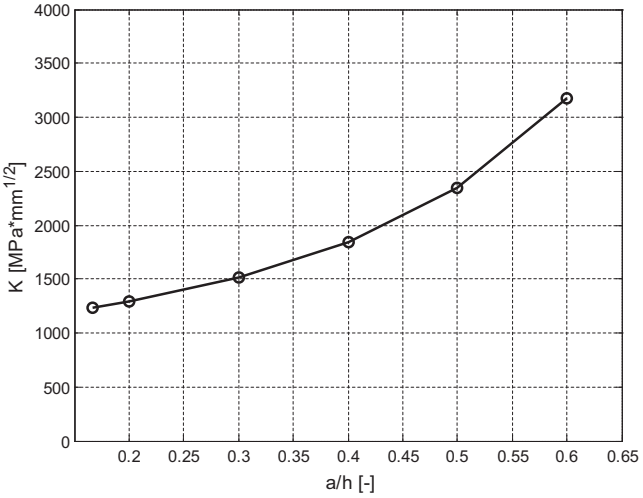


**Fig. 9.** Stress intensity factor of the bare steel beam ($P$ = 15 kN).

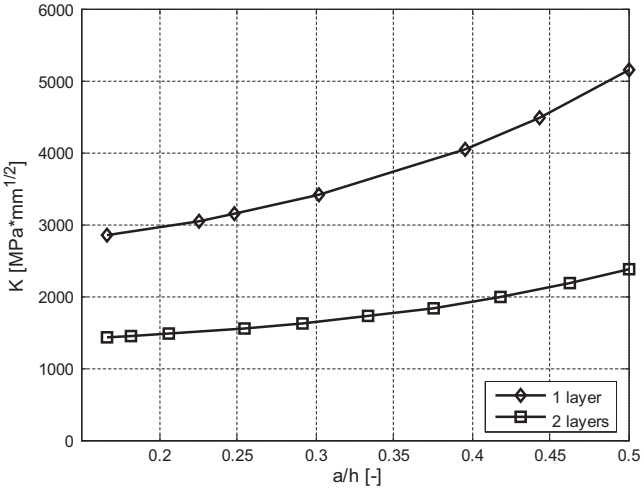


**Fig. 10.** Stress intensity factor of the reinforced steel beams ($P$ = 70 kN).

For the reinforced beams, the SIF was evaluated according to Eq. (15) for the maximum load level of 70 kN (see Table 1). In Fig. 10 the SIF was plotted as function of the normalized crack length, $a/h$.

Fig. 10 shows that the stress intensity factor strongly depends on the number of the reinforcement strips. The higher the reinforcement thickness, the higher the compressive force in the steel beam and then the lower the stress intensity factor (see Eq. (15)). In particular, the double reinforcement configuration exhibited a stress intensity factor which was less than 50% of the value reached for the single reinforcement configuration. This had a significant influence on the fatigue crack growth curve, as documented in the next section.

### *4.3. Fatigue life prediction*

The predicted fatigue crack growth curve, that is, the number of fatigue cycles, $N$, to attain a given crack size, $a$, was evaluated by the numerical integration of Eq. (1) as:

$$N(a) = \int_{a_i}^{a} \frac{da}{C \cdot \left(\Delta K_{eff}^{m} - \Delta K_{eff,th}^{m}\right)} \tag{17}$$

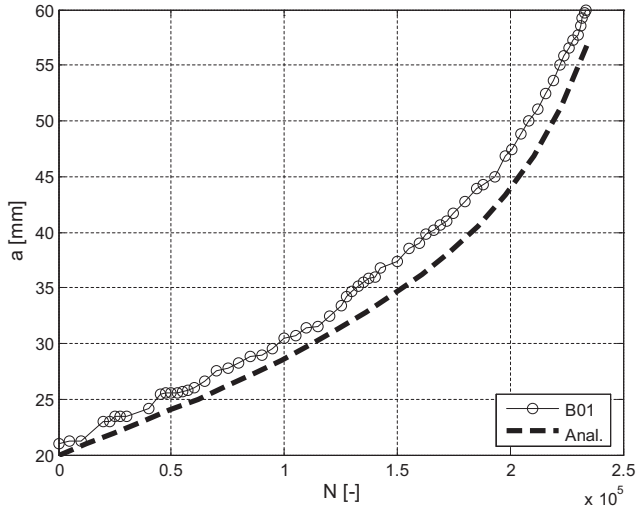


**Fig. 11.** Fatigue crack growth results: crack propagation curves and analytical modelling for the bare specimen ($P$ = 6–15 kN).

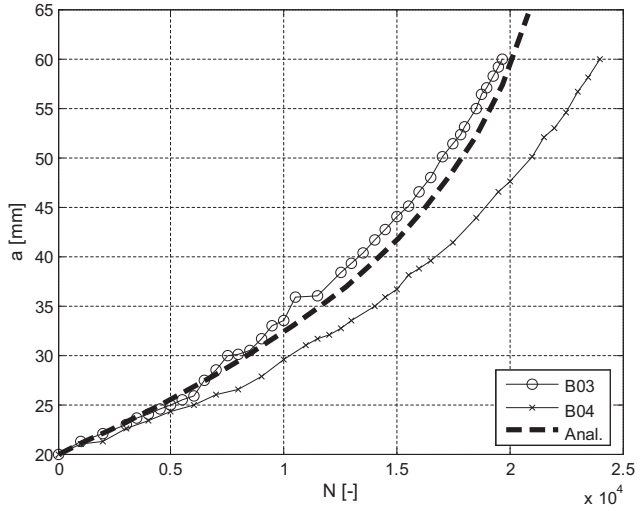


**Fig. 12.** Fatigue crack growth results: crack propagation curves and analytical modelling for the single reinforcement layer ($P$ = 28–70 kN).

where $C$, $m$ and $\Delta K_{eff,th}$ are the Paris constants listed in Table 2, $a_i$ is the initial crack size and $\Delta K_{eff}$ is the effective SIF range (see Eq. (2)). The Paris law was integrated between the initial crack size $a_i$ and a given crack size $a$. In particular, the effective load ratio $q$ was evaluated by means of Eq. (2) with an experimental corrector factor $\beta$ = 1.10. This value was estimated in [23] in order to achieve the best fit between experimental findings and analytical outcomes.

Results of the numerical integration of the fatigue crack growth law are reported in Figs. 11 and 12 for the unreinforced steel beam and for the steel beams with a single reinforcement layer, respectively. A satisfactory agreement between the experimental findings and the analytical results was observed.

Results for the double reinforcement layer are reported in Fig. 13.

In this case, the presence of a non-uniform distribution of the tensile force in the CFRP reinforcement (see Fig. 6) leads to a significant scatter of the fatigue crack growth curves. The fatigue crack growth rate is, in fact, very sensitive to the tensile force in the CFRP strips.

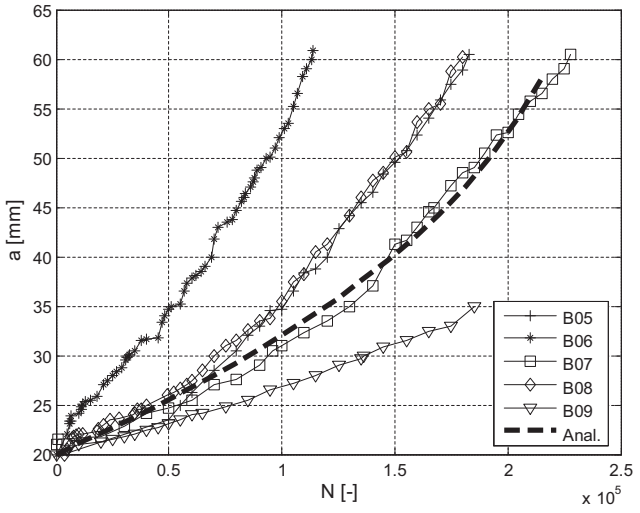


**Fig. 13.** Fatigue crack growth results: crack propagation curves and analytical modelling for the double reinforcement layer ($P$ = 28–70 kN).

## 5. Conclusions

The outcomes of the experimental campaign and the results of the analytical model developed for the prediction of the fatigue crack growth of steel beams reinforced with CFRP strips can be summarizes as follows:

- The strain gauges measurements show a strain concentration in the CFRP reinforcement at the cracked section. The axial force distribution in the composite strips is uniform for the single reinforcement configuration while it increases with the crack size, up to a crack size approximately equal to 25 mm, for the case of two reinforcement layers. When the crack size increases, the strain distribution becomes uniform for the double reinforcement, too. These results are in agreement with the observed fatigue crack growth rate.
- The strain gauges measurements also exhibit reinforcement debonding from the substrate at the cracked section, showing that the fatigue crack propagation is strictly related and influenced by the progressive debonding occurring at the interface between the reinforcement and the steel beam. The phenomenon is much more evident for the single reinforcement case and less clear, but still present and noticeable, for the double reinforcement case.
- One of the most important and innovative issues presented in this paper is the analytical model discussed in Section 3. The proposed model accurately calculates the strain distribution in the CFRP reinforcement for both the single and double reinforcement configurations. Besides, the adhesion model precisely predicts the tensile force in the CFRP strip for the single reinforcement layer and produces a reasonable estimation for the double reinforcement case.
- The proposed analytical model is also extremely useful since it correctly estimates the stress intensity factor for both the single and double reinforcement cases. Due to the reinforcement debonding at the cracked section, the axial force under the cracked section is assumed to be equal to the debonding force. In particular, the use of a double reinforcement configuration leads to a significant decrement of the stress intensity factor compared to the single layer case.
- Moreover, the analytical model was introduced for assessing the evaluation of the fatigue crack growth curves. The model takes into account the retardation effect and accurately predicts the fatigue crack growth of the bare and the single reinforcement steel beam case.
- Finally, it must be noticed that the fatigue crack growth for the double reinforcement case is a very complex phenomenon and a significant scatter of the fatigue crack propagation curves is due to the non-uniform stress redistribution between the CFRP strips and the steel beam. Nonetheless, analytical results show that even in this case the proposed mathematical model is capable to capture the mean fatigue crack growth behaviour.

## Acknowledgements

The experimental tests were performed at the Material Testing Laboratory of the Politecnico di Milano. The financial support of the Politecnico di Milano is also gratefully acknowledged. Thanks are also expressed to Sika Italia S.p.A. for providing the pultruded strips and the epoxy adhesive used in the experimental program.

## References

[1] H.A. Jiao, F. Mashiri, X.L. Zhao, A comparative study on fatigue behaviour of steel beams retrofitted with welding, pultruded CFRP plates and wet layup CFRP sheets, Thin Walled Struct. 59 (2012) 144–152.
[2] L.C. Hollaway, J. Cadei, Progress in the technique of upgrading metallic structures with advanced polymer composites, Prog. Struct. Eng. Mater. 4 (2) (2002) 131–148.
[3] X.L. Zhao, L. Zhang, State of the art review on FRP strengthened steel structures, Eng. Struct. 29 (8) (2007) 1808–1823.
[4] J.G. Teng, T. Yu, D. Fernando, Strengthening of steel structures with fiber-reinforced polymer composites, J. Constr. Steel Res. 78 (2012) 131–143.
[5] X.L. Zhao, FRP strengthening of metallic structures subject to fatigue loading, in: Proceedings of Seventh National Conference on FRP in Construction, Hangzhou, China, October 2011, pp. 15–16.
[6] J.M.C. Cadei, T.J. Stratford, L.C. Hollaway, W.H. Duckett, C595-Strengthening Metallic Structures using Externally Bonded Fibre-Reinforced Composites, CIRIA, London, 2004.
[7] D. Schnerch, M. Dawood, S. Rizkalla, E. Sumner, Proposed design guidelines for strengthening of steel bridges with FRP materials, Constr. Build. Mater. 21 (5) (2007) 1001–1010.
[8] K. Nozaka, C.K. Shield, J.F. Hajjar, Effective bond length of carbon-fiber-reinforced polymer strips bonded to fatigue steel bridge I-girders, J. Bridge Eng. 10 (2) (2005) 195–205.
[9] J. Deng, M.M.K. Lee, Fatigue performance of metallic beam strengthened with a bonded CFRP plate, Compos. Struct. 78 (2007) 222–231.
[10] E. Ghafoori, M. Motavalli, Analytical calculation of stress intensity factor of cracked steel I-beams with experimental analysis and 3D digital image correlation measurements, Eng. Fract. Mech. 78 (2011) 3226–3242.
[11] Y.J. Kim, K.A. Harries, Fatigue behaviour of damaged steel beams repaired with CFRP strips, Eng. Struct. 33 (5) (2011) 1491–1502.
[12] A. Hmidan, Y.J. Kim, S. Yazdani, CFRP repair of steel beams with various initial crack configurations, J. Compos. Constr. 15 (6) (2011) 952–963.
[13] A. Hmidan, Y.J. Kim, S. Yazdani, Stress intensity factors for cracked steel girders strengthened with CFRP sheets, J. Compos. Constr. (2014), http://dx.doi.org/10.1061/(ASCE)CC.1943-5614.0000552.
[14] Y.J. Kim, G. Brunell, Interaction between CFRP-repair and initial damage of wide-flange steel beams subjected to three-point bending, Compos. Struct. 93 (8) (2011) 1986–1996.
[15] E. Ghafoori, M. Motavalli, J. Botsis, A. Herwig, M. Galli, Fatigue Strengthening of damaged metallic beams using prestressed unbonded and bonded CFRP plates, Int. J. Fatigue 44 (2012) 303–315.
[16] E. Ghafoori, A. Schumacher, M. Motavalli, Fatigue behavior of notched steel beams reinforced with bonded CFRP plates: determination of prestressing level for crack arrest, Eng. Struct. 45 (2012) 270–283.
[17] Y.J. Kim, K.A. Harries, Predictive response of notched steel beams repaired with CFRP strips including bond-slip behaviour, Int. J. Struct. Stab. Dy. 12 (1) (2012) 1–21.
[18] G. Wu, H.T. Wang, Z.S. Wu, H.Y. Liu, Y. Ren, Experimental study on the fatigue behavior of steel beams strengthened with different fiber-reinforced composite plates, J. Compos. Constr. 16 (2) (2012) 127–137.
[19] E. Ghafoori, M. Motavalli, A. Nussbaumer, A. Herwig, G.S. Prinz, M. Fontana, Determination of minimum CFRP pre-stress levels for fatigue crack prevention in retrofitted metallic beams, Eng. Struct. 84 (2015) 29–41.

[20] E. Ghafoori, M. Motavalli, A. Nussbaumer, A. Herwig, G.S. Prinz, M. Fontana, Design criterion for fatigue strengthening of riveted beams in a 120-year-old railway metallic bridge using pre-stressed CFRP plates, Compos. B Eng. 68 (2015) 1–13.
[21] P. Colombi, G. Fava, Fatigue life of steel components strengthened with fibre-reinforced polymer (FRP) composites, in: V.M. Karbhari (Ed.), Rehabilitation of Metallic Civil Infrastructure using Fiber Reinforced Polymer (FRP) Composites, Woodhead, Cambridge, 2014, pp. 239–268.
[22] P. Colombi, G. Fava, Experimental study on the fatigue behavior of cracked steel beams repaired with CFRP plates, Eng. Fract. Mech. 145 (2015) 128–142.
[23] P. Colombi, G. Fava, L. Sonzogni, Fatigue crack growth in CFRP-strengthened steel plates, Compos. B Eng. 72 (2015) 87–96.
[24] D. Broek, Elementary Engineering Fracture Mechanics, Martinus Nijhoff Publishers, The Hague, The Netherlands, 1982.
[25] M.L. Dunn, W. Suwito, B. Hunter, Stress intensity factors for cracked I-beams, Eng. Fract. Mech. 57 (6) (1997) 609–615.